DOI: 10.7511/jslx20230909001

An advanced computational approach for layered structure modeling

PAN Er-nian*[1], ZHOU Jiang-cun[2],
LIN Chih-ping[1], ZHANG Zhi-qing[3]

(1. Civil Engineering and Disaster Prevention & Water Environment Research Center, Yang Ming Chiao Tung University, Hsinchu 300, China;
2. State Key Laboratory of Geodesy and Earth's Dynamics, Innovation Academy for Precision Measurement Science and Technology, Chinese Academy of Sciences, Wuhan 430077, China;
3. College of Architecture and Energy Engineering, Wenzhou University of Technology, Zhejiang 325035, China)

Abstract: In this paper, we present an advanced computational approach for modeling layered structures. The structures can be horizontally layered plates or layered half-spaces. The materials can be multi-field coupled, i.e., thermoelastic, poroelastic, and magnetoelectroelastic coupled, but require that they are transversely isotropic (TI) with material symmetry axis along the layering direction. This advanced approach is based on the recently constructed Fourier-Bessel series (FBS) system of vector functions and the dual-variable and position (DVP) method. While the DVP is for propagating the layer matrix from one layer to the next with unconditional stability, the FBS vector system is to 1) represent the general deformations/waves with distinguished deformation/wave types, and 2) pre-calculate the expansion coefficients as Love numbers and then use them later for massive simulation of the involved problem. Three typical examples are presented to demonstrate the accuracy and efficiency, as compared with the existing approaches. These are: faulting (or dislocation) in a layered earth, soil-structure interaction, and transient wave propagation in a near-surface earth profile.

Key words: layered media; transverse isotropy; Fourier-Bessel series system; dual-variable and position method; multi-field coupling; Love number

1 Introduction

In nature, many systems present themselves in layered structures: Our global Earth is approximately a spherical and layered body. In its regional scale, we have a horizontally layered half-space. Civil engineers are also often faced with layered half-spaces in their daily research and design. Learned from nature, manmade layered structures are reported from time to time, with excellent physical properties.

When solving the boundary-value problems in the layered structures, the domain-discretization method, boundary-discretization method, and the related hybrid method were proposed[1,2]. If the layers are horizontal with material properties in each layer being uniform, analytical solutions can be derived[3]. The common approach is to apply either the two-dimensional (2D) Fourier-transform (for general deformation/wave) or Hankel transform (for axis-symmetric geometry, as in Ref.[4-7]) to suppress the horizontal dependences in the governing equations.

Instead of the scalar 2D Fourier transform or one-dimensional (1D) Hankel transform, both Cartesian system and cylindrical system of vector functions can be applied[8-10]. The advantages of applying these systems of vector functions are: the dilatational and torsional deformations are clearly decoupled. For wave motion, this means that the P-SV/Rayleigh waves

Received by: 2023-09-09; **Revised by**: 2023-10-30.
Project supported by NSTC 111-2811-E-A49-534; Open Fund of Hubei Luojia Laboratory (220100033); Ministry of Science and Technology of Taiwan (MOST 110-2625-M-A49-004); National Natural Science Foundation of China(52178367).
Corresponding authors: PAN Er-nian* (1955-), Male, Professor (E-mail: ernianpan@nycu.edu.tw).

and SH/Love waves are decoupled. Therefore, in terms of these vector functions, not only the governing equations are decoupled but also these decoupled equations are directly physically connected. In other words, once the loading or source type is given, then the corresponding decoupled governing equations can be applied to find the solution.

For the axis-symmetric case, once the solutions are obtained in the Hankel transformed domain, we need to apply the inverse transform to find the corresponding physical-domain solution. This is usually carried out by the numerical quadrature with perhaps the most accurate and fast one being the MATLAB code[11] developed based on the mathematical formulations presented by Lucas and his coauthor[12,13]. However, it is still very computationally intensive in most applications.

Another approach is to replace the Hankel integral transform by the Fourier-Bessel series (FBS) expansion[14], as inspired from the spectral element method[15]. Compared to the Hankel integral transform, this series approach is computationally more efficient for a given accuracy[16,17]. This is due to the fact that, the FBS method requires only simple summation over discrete zero points of the Bessel functions, whilst the inverse Hankel integral transform has to be numerically carried out over each interval between these zero points. Another important advantage which should be particularly emphasized is that the expansion coefficients in terms of the FBS are discrete, and as such, they can be called Love numbers similar to those in the layered spherical Earth[18]. Since these Love numbers are discrete, they can be pre-calculated and saved for later use as have been frequently applied in geophysics[19], substantially reducing the computational cost. While the FBS expansion is very efficient and accurate, it was limited to the simple symmetric vertical loading case only. Recently, Pan et al.[20] constructed a complete vector system from the FBS, called FBS system of vector functions. Based on this vector system, any vector as well as scalar function can be expanded so that the very general boundary-value problem in layered structures can be solved.

In the transformed domain, we will have a system of ordinary differential equations (with respect to the thickness z variable). This system of equations can be solved in each layer and then various matrix methods can be applied to propagate the solutions from one layer to the next[3]. The common ones are the traditional propagation matrix method, also called the Thomson—Haskell method[21,22], the reflection and transmission matrix method[23], the stiffness matrix method[24]. Recently, a very powerful method, called the dual-variable and position (DVP) method[25,26] was proposed rooted from the precision integration method[27]. We point out that a similar formulation, called compliance-stiffness matrix method, was proposed with applications in electric engineering[28].

In this paper, we briefly review the novel approach we recently developed for handling layered structures: The FBS system of vector functions combined with the DVP method. Its accuracy and efficiency will be illustrated via three typical engineering/science examples: Faulting (or dislocation) in a layered earth, soil-structure interactions, and transient waves in near-surface earth profiles.

2 Boundary-value problem and basic solutions

We use purely elastic materials to illustrate the algorithm. We assume that there is a q-layered transversely isotropic (TI) elastic structure where the last layer could be a rigid base or a homogeneous TI half-space. We place the $z=0$ plane on the surface of the layered structures with positive z pointing down to the medium. The layers are ordered from top down, with layer l being bonded on its upper interface at $z=z_{l-1}$ and its lower interface at $z=z_l$, with a thickness $h_l=z_l-z_{l-1}$. As such, the upper interface of the first layer is at the surface of the layered structure at $z=z_0=0$, and the last interface is at $z=z_q$. The concentrated source can be either a force or a dislocation (fault for earthquake simulation), applied, e.g., at $z=z_s$ in layer j. The special case is the source on the surface with $z_s=z_0=0$. Due to the applied force or dislocation, the displacements and tractions (at $z=z_s$) will become discontinuous. Except for this source

level, we assume that the displacements and tractions are continuous on all the interfaces. Notice that imperfect interface conditions can be considered if needed[25,26].

In order to solve the problem, the following steps can be applied.

Step 1 to get rid of the time-dependence. For the transient (time-harmonic as an example) case, we first apply the Fourier transform to suppress the time-derivative so that only the space-variation is involved. The governing equations are well known, as listed below[25,26]

$$\frac{\partial \sigma_{rr}}{\partial r}+\frac{1}{r}\frac{\partial \sigma_{r\theta}}{\partial \theta}+\frac{\partial \sigma_{rz}}{\partial z}+\frac{\sigma_{rr}-\sigma_{\theta\theta}}{r}+f_r=-\rho\omega^2 u_r$$

$$\frac{\partial \sigma_{r\theta}}{\partial r}+\frac{1}{r}\frac{\partial \sigma_{\theta\theta}}{\partial \theta}+\frac{\partial \sigma_{\theta z}}{\partial z}+\frac{2\sigma_{r\theta}}{r}+f_\theta=-\rho\omega^2 u_\theta$$

$$\frac{\partial \sigma_{rz}}{\partial r}+\frac{1}{r}\frac{\partial \sigma_{\theta z}}{\partial \theta}+\frac{\partial \sigma_{zz}}{\partial z}+\frac{\sigma_{rz}}{r}+f_z=-\rho\omega^2 u_z \tag{1}$$

$$\sigma_{rr}=c_{11}\varepsilon_{rr}+c_{12}\varepsilon_{\theta\theta}+c_{13}\varepsilon_{zz}$$

$$\sigma_{\theta\theta}=c_{12}\varepsilon_{rr}+c_{11}\varepsilon_{\theta\theta}+c_{13}\varepsilon_{zz}$$

$$\sigma_{zz}=c_{13}\varepsilon_{rr}+c_{13}\varepsilon_{\theta\theta}+c_{33}\varepsilon_{zz}$$

$$\sigma_{r\theta}=2c_{66}\varepsilon_{r\theta},\ \sigma_{\theta z}=2c_{44}\varepsilon_{\theta z},\ \sigma_{rz}=2c_{44}\varepsilon_{rz} \tag{2}$$

$$\varepsilon_{rr}=\frac{\partial u_r}{\partial r},\ \varepsilon_{\theta\theta}=\frac{\partial u_\theta}{r\partial\theta}+\frac{u_r}{r},\ \varepsilon_{zz}=\frac{\partial u_z}{\partial z}$$

$$\varepsilon_{r\theta}=0.5\left(\frac{\partial u_r}{r\partial\theta}+\frac{\partial u_\theta}{\partial r}-\frac{u_\theta}{r}\right)$$

$$\varepsilon_{\theta z}=0.5\left(\frac{\partial u_\theta}{\partial z}+\frac{\partial u_z}{r\partial\theta}\right),\ \varepsilon_{rz}=0.5\left(\frac{\partial u_z}{\partial r}+\frac{\partial u_r}{\partial z}\right) \tag{3}$$

Step 2 to get rid of the horizontal variables in the governing equations (1～3) above. For either axis-symmetric or general 3D deformation/wave (with the angular dependence in terms of different orders of triangular functions), traditionally we apply the Hankel transform of different orders. For instance, following Lin et al.[5] for the general loading case, one can expand the displacements as

$$\begin{aligned}u_r(r,\theta,z;m)&=\sum_m\left[u_r^s(r,z;m)\cos m\theta+\right.\\&\left.u_r^a(r,z;m)\sin m\theta\right]\\u_r(r,\theta,z;m)&=\sum_m\left[-u_\theta^s(r,z;m)\sin m\theta+\right.\\&\left.u_\theta^a(r,z;m)\cos m\theta\right]\\u_z(r,\theta,z;m)&=\sum_m\left[u_z^s(r,z;m)\cos m\theta+\right.\\&\left.u_z^a(r,z;m)\sin m\theta\right]\end{aligned} \tag{4}$$

where the involved expansion coefficients on the right-hand sides will be only functions of r and z (along with frequency-dependence). After that, the Hankel transform is applied to get rid of the r-dependence, by applying

$$\begin{aligned}\tilde{f}(k)&=\int_0^\infty f(r)\,J_m(kr)\,r\,dr\\f(r)&=\int_0^\infty \tilde{f}(k)\,J_m(kr)\,k\,dk\end{aligned} \tag{5}$$

Instead of Eqs.(4,5), the following cylindrical system of vector functions(CSVF) can be applied[8,9]

$$\begin{aligned}\mathbf{L}(r,\theta;\lambda,m)&=\boldsymbol{e}_z S(r,\theta;\lambda,m)\\\mathbf{M}(r,\theta;\lambda,m)&=\left(\boldsymbol{e}_r\frac{\partial}{\partial r}+\boldsymbol{e}_\theta\frac{\partial}{r\partial\theta}\right)S(r,\theta;\lambda,m)\\\mathbf{N}(r,\theta;\lambda,m)&=\left(\boldsymbol{e}_r\frac{\partial}{r\partial\theta}-\boldsymbol{e}_\theta\frac{\partial}{\partial r}\right)S(r,\theta;\lambda,m)\end{aligned} \tag{6}$$

$$S(r,\theta;\lambda,m)=\frac{1}{\sqrt{2\pi}}J_m(\lambda r)e^{im\theta};\ m=0,\pm1,\pm2,\cdots \tag{7}$$

where $\boldsymbol{e}_r,\boldsymbol{e}_\theta,\boldsymbol{e}_z$ are the unit vectors along the coordinate axes r, θ, z, respectively; $J_m(\lambda r)$ denotes the Bessel function of order m; and λ is the transform variable. Notice that the CSVF is an extension of the scalar Hankel transform to the vector form, and it further processes certain merits to be discussed below.

Since the vector system defined in Eq.(6) is orthonormal, the displacement vector $\boldsymbol{u}$ and the traction vector t (at $z=$constant), can be expanded as

$$\begin{aligned}\boldsymbol{u}(r,\theta,z)=\sum_m\int_0^{+\infty}&\left[U_L(z)\mathbf{L}(r,\theta;\lambda,m)+\right.\\&U_M(z)\mathbf{M}(r,\theta;\lambda,m)+\\&\left.U_N(z)\mathbf{N}(r,\theta;\lambda,m)\right]\lambda\,d\lambda\end{aligned} \tag{8}$$

$$\begin{aligned}\boldsymbol{t}(r,\theta,z)\equiv\sigma_{rz}\boldsymbol{e}_r+\sigma_{\theta z}\boldsymbol{e}_\theta+\sigma_{zz}\boldsymbol{e}_z=&\\\sum_m\int_0^{+\infty}&\left[T_L(z)\mathbf{L}(r,\theta;\lambda,m)+\right.\\&T_M(z)\mathbf{M}(r,\theta;\lambda,m)+\\&\left.T_N(z)\mathbf{N}(r,\theta;\lambda,m)\right]\lambda\,d\lambda\end{aligned} \tag{9}$$

where U_i and T_i $(i=L,M,N)$ are the expansion coefficients of the displacement and traction vectors, respectively; Notice that the body force and any given tractions can be also expanded. This CSVF has been used for many near-surface geophysics, soil-structure interaction, and earthquake engineering problems. The beauty and physics connections are the decomposition of different types of deformations or waves.

The advantages of applying these systems of vector functions are[8-10]: The dilatational and torsional deformations are clearly decoupled. For the wave case, it means that the P-SV/Rayleigh waves and SH/Love waves are decoupled. Therefore,

in terms of these vector functions, not only the governing equations are decoupled but also these decoupled equations are directly physically connected.

Very recently, a computationally very efficient vector system, i.e., the FBS vector functions, was proposed, as defined below[20]

$$\mathbf{L}(r,\theta;m,k)=\boldsymbol{e}_z \mathrm{S}(r,\theta;m,k)$$

$$\mathbf{M}(r,\theta;m,k)=\left(\boldsymbol{e}_r\frac{\partial}{\partial r}+\boldsymbol{e}_\theta\frac{\partial}{r\partial\theta}\right)\mathrm{S}(r,\theta;m,k)$$

$$\mathbf{N}(r,\theta;m,k)=\left(\boldsymbol{e}_r\frac{\partial}{r\partial\theta}-\boldsymbol{e}_\theta\frac{\partial}{\partial r}\right)\mathrm{S}(r,\theta;m,k) \quad (10)$$

$$\mathrm{S}(r,\theta;m,k)=\frac{1}{\sqrt{2\pi}}J_m(\lambda_{mk}r)\,\boldsymbol{e}^{im\theta} \quad (11)$$

where λ_{mk} is the k^{th} zero of the Bessel function of order m, J_m, scaled by a large value of R, i.e., $J_m(\lambda_{mk}R)=0$. Hence, the displacement and traction vectors can be expanded as

$$\begin{aligned}\boldsymbol{u}(r,\theta,z)=u_z\boldsymbol{e}_z+u_r\boldsymbol{e}_r+u_\theta\boldsymbol{e}_\theta=\\ \sum_m\sum_k\big[&\mathrm{U_L}(\lambda_{mk},z)\mathbf{L}(r,\theta;m,k)+\\ &\mathrm{U_M}(\lambda_{mk},z)\mathbf{M}(r,\theta;m,k)+\\ &\mathrm{U_N}(\lambda_{mk},z)\mathbf{N}(r,\theta;m,k)\big]\end{aligned} \quad (12)$$

$$\begin{aligned}\boldsymbol{t}(r,\theta,z)=\sigma_{zz}\boldsymbol{e}_z+\sigma_{zr}\boldsymbol{e}_r+\sigma_{z\theta}\boldsymbol{e}_\theta=\\ \sum_m\sum_k\big[&\mathrm{T_L}(\lambda_{mk},z)\mathbf{L}(r,\theta;m,k)+\\ &\mathrm{T_M}(\lambda_{mk},z)\mathbf{M}(r,\theta;m,k)+\\ &\mathrm{T_N}(\lambda_{mk},z)\mathbf{N}(r,\theta;m,k)\big]\end{aligned} \quad (13)$$

Then, in terms of the FBS vector functions, the governing equations (1～3) can be reduced to the following linear systems of ordinary differential equations in each material layer, as listed below[20].

For the N-type

$$\frac{\mathrm{d}}{\mathrm{d}z}\begin{bmatrix}\lambda_{mk}\mathrm{U_N}\\ \mathrm{T_N}\end{bmatrix}=\lambda_{mk}\begin{bmatrix}0 & 1/c_{44}\\ c_{66}-\rho\omega^2/\lambda_{mk}^2 & 0\end{bmatrix}\begin{bmatrix}\lambda_{mk}\mathrm{U_N}\\ \mathrm{T_N}\end{bmatrix} \quad (14)$$

For the *LM*-type

$$\frac{\mathrm{d}}{\mathrm{d}z}\begin{bmatrix}\mathrm{U_L}\\ \lambda_{mk}\mathrm{U_M}\\ \dfrac{\mathrm{T_L}}{\lambda_{mk}}\\ \mathrm{T_M}\end{bmatrix}=\lambda_{mk}\begin{bmatrix}0 & \dfrac{c_{13}}{c_{33}} & \dfrac{1}{c_{33}} & 0\\ -1 & 0 & 0 & \dfrac{1}{c_{44}}\\ -\dfrac{\rho\omega^2}{\lambda_{mk}^2} & 0 & 0 & 1\\ 0 & \dfrac{c_{11}c_{33}-c_{13}^2}{c_{33}} & -\dfrac{\rho\omega^2}{\lambda_{mk}^2} & -\dfrac{c_{13}}{c_{33}} & 0\end{bmatrix}\times\begin{bmatrix}\mathrm{U_L}\\ \lambda_{mk}\mathrm{U_M}\\ \dfrac{\mathrm{T_L}}{\lambda_{mk}}\\ \mathrm{T_M}\end{bmatrix} \quad (15)$$

We define the following two vectors

$$\begin{aligned}\mathbf{U}(z)&=\left[\mathrm{U_L}(z)\quad \lambda_{mk}\mathrm{U_M}(z)\right]^t\\ \mathbf{T}(z)&=\left[\mathrm{T_L}(z)/\lambda_{mk}\quad \mathrm{T_M}(z)\right]^t\end{aligned} \quad (16)$$

Now, for the given problem with the source in layer j (traction free on the surface $z=z_0$), we subdivide the source layer into two sublayers as $j1$ and $j2$, with their thickness being $h_{s1}=z_s-z_{j-1}$ and $h_{s2}=z_j-z_s$. We then propagate from the surface to the upper side of the source z_{s-}, and from the lower side of the source z_{s+} to the last interface to arrive at Ref.[29,30]

$$\begin{bmatrix}\lambda_{mk}\mathrm{U_N}(z_0)\\ \mathrm{T_N}(z_{s-})\end{bmatrix}=\begin{bmatrix}\mathrm{N}_{11}^{1;j1} & \mathrm{N}_{12}^{1;j1}\\ \mathrm{N}_{21}^{1;j1} & \mathrm{N}_{22}^{1;j1}\end{bmatrix}\begin{bmatrix}\lambda_{mk}\mathrm{U_N}(z_{s-})\\ \mathrm{T_N}(z_0)\end{bmatrix} \quad (17)$$

$$\begin{bmatrix}\mathbf{U}(z_0)\\ \mathbf{T}(z_{s-})\end{bmatrix}=\begin{bmatrix}\mathbf{S}_{11}^{1;j1} & \mathbf{S}_{12}^{1;j1}\\ \mathbf{S}_{21}^{1;j1} & \mathbf{S}_{22}^{1;j1}\end{bmatrix}\begin{bmatrix}\mathbf{U}(z_{s-})\\ \mathbf{T}(z_0)\end{bmatrix} \quad (18)$$

$$\begin{bmatrix}\lambda_{mk}\mathrm{U_N}(z_{s+})\\ \mathrm{T_N}(z_q)\end{bmatrix}=\begin{bmatrix}\mathrm{N}_{11}^{j2;q} & \mathrm{N}_{12}^{j2;q}\\ \mathrm{N}_{21}^{j2;q} & \mathrm{N}_{22}^{j2;q}\end{bmatrix}\begin{bmatrix}\lambda_{mk}\mathrm{U_N}(z_q)\\ \mathrm{T_N}(z_{s+})\end{bmatrix} \quad (19)$$

$$\begin{bmatrix}\mathbf{U}(z_{s+})\\ \mathbf{T}(z_q)\end{bmatrix}=\begin{bmatrix}\mathbf{S}_{11}^{j2;q} & \mathbf{S}_{12}^{j2;q}\\ \mathbf{S}_{21}^{j2;q} & \mathbf{S}_{22}^{j2;q}\end{bmatrix}\begin{bmatrix}\mathbf{U}(z_q)\\ \mathbf{T}(z_{s+})\end{bmatrix} \quad (20)$$

Thus, for the given discontinuities (or the source functions) at the source level $z=z_s$, Eqs.(18～20) can be arranged for solving the expansion coefficients. Taking the case where only forces are applied at $z=z_s$ and the surface is traction-free (i.e., Ref.[29,30]), we have,

$$\begin{aligned}\begin{bmatrix}\lambda_{mk}\mathrm{U_N}(z_0)\\ \lambda_{mk}\mathrm{U_N}(z_s)\\ \mathrm{T_N}(z_{s-})\\ \lambda_{mk}\mathrm{U_N}(z_q)\end{bmatrix}=&\begin{bmatrix}-1 & \mathrm{N}_{11}^{1;j1} & 0 & 0\\ 0 & \mathrm{N}_{21}^{1;j1} & -1 & 0\\ 0 & -1 & \mathrm{N}_{12}^{j2;q} & \mathrm{N}_{11}^{j2;q}\\ 0 & 0 & \mathrm{N}_{22}^{j2;q} & \mathrm{N}_{21}^{j2;q}-\mathrm{E}_{\mathrm{N}22}^{q+1}(\mathrm{E}_{\mathrm{N}12}^{q+1})^{-1}\end{bmatrix}^{-1}\times\\ &\begin{bmatrix}0\\ 0\\ -\mathrm{N}_{12}^{j2;q}\Delta\mathrm{T_N}(z_s)\\ -\mathrm{N}_{22}^{j2;q}\Delta\mathrm{T_N}(z_s)\end{bmatrix}\end{aligned} \quad (21)$$

$$\begin{aligned}\begin{bmatrix}\mathbf{U}(z_0)\\ \mathbf{U}(z_s)\\ \mathbf{T}(z_{s-})\\ \mathbf{U}(z_q)\end{bmatrix}=&\begin{bmatrix}-\boldsymbol{I} & \mathbf{S}_{11}^{1;j1} & \mathbf{0} & \mathbf{0}\\ \mathbf{0} & \mathbf{S}_{21}^{1;j1} & -\boldsymbol{I} & \mathbf{0}\\ \mathbf{0} & -\boldsymbol{I} & \mathbf{S}_{12}^{j2;q} & \mathbf{S}_{11}^{j2;q}\\ \mathbf{0} & \mathbf{0} & \mathbf{S}_{22}^{j2;q} & \mathbf{S}_{21}^{j2;q}-\mathbf{E}_{22}^{q+1}(\mathbf{E}_{12}^{q+1})^{-1}\end{bmatrix}^{-1}\times\\ &\begin{bmatrix}\mathbf{0}\\ \mathbf{0}\\ -\mathbf{S}_{12}^{j2;q}\Delta\mathbf{T}(z_s)\\ -\mathbf{S}_{22}^{j2;q}\Delta\mathbf{T}(z_s)\end{bmatrix}\end{aligned} \quad (22)$$

where the scalar functions and submatrices with superscript $q+1$ denote the eigenvectors in the last

homogeneous half-space[25,26]. Notice that here the discontinuity is for the traction only; the corresponding dislocation source can be equally studied, as in Ref.[18]. After that, depending on the relative locations of the field points, we can solve for the field quantities at any depth.

If $z_f < z_s$: We propagate the layer matrix from the surface z_0 to z_f and then from z_f to z_{s-} on the upper side of the source to have

$$\begin{bmatrix}\lambda_{mk}U_N(z_0)\\ T_N(z_f)\end{bmatrix}=\begin{bmatrix}N_{11}^{1:kf} & N_{12}^{1:kf}\\ N_{21}^{1:kf} & N_{22}^{1:kf}\end{bmatrix}\begin{bmatrix}\lambda_{mk}U_N(z_f)\\ 0\end{bmatrix} \tag{23}$$

$$\begin{bmatrix}\boldsymbol{U}(z_0)\\ \boldsymbol{T}(z_f)\end{bmatrix}=\begin{bmatrix}\boldsymbol{S}_{11}^{1:kf} & \boldsymbol{S}_{12}^{1:kf}\\ \boldsymbol{S}_{21}^{1:kf} & \boldsymbol{S}_{22}^{1:kf}\end{bmatrix}\begin{bmatrix}\boldsymbol{U}(z_f)\\ \boldsymbol{0}\end{bmatrix} \tag{24}$$

$$\begin{bmatrix}\lambda_{mk}U_N(z_f)\\ T_N(z_{s-})\end{bmatrix}=\begin{bmatrix}N_{11}^{kf:j1} & N_{12}^{kf:j1}\\ N_{21}^{kf:j1} & N_{22}^{kf:j1}\end{bmatrix}\begin{bmatrix}\lambda_{mk}U_N(z_s)\\ T_N(z_f)\end{bmatrix} \tag{25}$$

$$\begin{bmatrix}\boldsymbol{U}(z_f)\\ \boldsymbol{T}(z_{s-})\end{bmatrix}=\begin{bmatrix}\boldsymbol{S}_{11}^{kf:j1} & \boldsymbol{S}_{12}^{kf:j1}\\ \boldsymbol{S}_{21}^{kf:j1} & \boldsymbol{S}_{22}^{kf:j1}\end{bmatrix}\begin{bmatrix}\boldsymbol{U}(z_s)\\ \boldsymbol{T}(z_f)\end{bmatrix} \tag{26}$$

Hence the solutions of the expansion coefficients at the field level, along with other quantities, can be expressed as

$$\begin{bmatrix}\lambda_{mk}U_N(z_0)\\ \lambda_{mk}U_N(z_f)\\ T_N(z_f)\\ \lambda_{mk}U_N(z_s)\end{bmatrix}=\begin{bmatrix}-1 & N_{11}^{1:kf} & 0 & 0\\ 0 & N_{21}^{1:kf} & -1 & 0\\ 0 & -1 & N_{12}^{kf:j1} & N_{11}^{kf:j1}\\ 0 & 0 & N_{22}^{kf:j1} & N_{21}^{kf:j1}\end{bmatrix}^{-1}\begin{bmatrix}0\\ 0\\ 0\\ T_N(z_{s-})\end{bmatrix} \tag{27}$$

$$\begin{bmatrix}\boldsymbol{U}(z_0)\\ \boldsymbol{U}(z_f)\\ \boldsymbol{T}(z_f)\\ \boldsymbol{U}(z_s)\end{bmatrix}=\begin{bmatrix}-\boldsymbol{I} & \boldsymbol{S}_{11}^{1:kf} & \boldsymbol{0} & \boldsymbol{0}\\ \boldsymbol{0} & \boldsymbol{S}_{21}^{1:kf} & -\boldsymbol{I} & \boldsymbol{0}\\ \boldsymbol{0} & -\boldsymbol{I} & \boldsymbol{S}_{12}^{kf:j1} & \boldsymbol{S}_{11}^{kf:j1}\\ \boldsymbol{0} & \boldsymbol{0} & \boldsymbol{S}_{22}^{kf:j1} & \boldsymbol{S}_{21}^{kf:j1}\end{bmatrix}^{-1}\begin{bmatrix}\boldsymbol{0}\\ \boldsymbol{0}\\ \boldsymbol{0}\\ \boldsymbol{T}(z_{s-})\end{bmatrix} \tag{28}$$

If $z_f > z_s$: We propagate the layer matrix from the lower side of the source z_s to z_f and then from z_f to z_q, to have

$$\begin{bmatrix}\lambda_{mk}U_N(z_s)\\ T_N(z_f)\end{bmatrix}=\begin{bmatrix}N_{11}^{j2:kf} & N_{12}^{j2:kf}\\ N_{21}^{j2:kf} & N_{22}^{j2:kf}\end{bmatrix}\begin{bmatrix}\lambda_{mk}U_N(z_f)\\ T_N(z_{s+})\end{bmatrix} \tag{29}$$

$$\begin{bmatrix}\boldsymbol{U}(z_s)\\ \boldsymbol{T}(z_f)\end{bmatrix}=\begin{bmatrix}\boldsymbol{S}_{11}^{j2:kf} & \boldsymbol{S}_{12}^{j2:kf}\\ \boldsymbol{S}_{21}^{j2:kf} & \boldsymbol{S}_{22}^{j2:kf}\end{bmatrix}\begin{bmatrix}\boldsymbol{U}(z_f)\\ \boldsymbol{T}(z_{s+})\end{bmatrix} \tag{30}$$

$$\begin{bmatrix}\lambda_{mk}U_N(z_f)\\ E_{22}^N(E_{12}^N)^{-1}U_N(z_q)\end{bmatrix}=\begin{bmatrix}N_{11}^{kf:q} & N_{12}^{kf:q}\\ N_{21}^{kf:q} & N_{22}^{kf:q}\end{bmatrix}\begin{bmatrix}\lambda_{mk}U_N(z_q)\\ T_N(z_f)\end{bmatrix} \tag{31}$$

$$\begin{bmatrix}\boldsymbol{U}(z_f)\\ [E_{22}E_{12}^{-1}]\boldsymbol{U}(z_q)\end{bmatrix}=\begin{bmatrix}\boldsymbol{S}_{11}^{kf:q} & \boldsymbol{S}_{12}^{kf:q}\\ \boldsymbol{S}_{21}^{kf:q} & \boldsymbol{S}_{22}^{kf:q}\end{bmatrix}\begin{bmatrix}\boldsymbol{U}(z_q)\\ \boldsymbol{T}(z_f)\end{bmatrix} \tag{32}$$

The solutions for the unknowns, including other coefficients, can be expressed as,

$$\begin{bmatrix}\lambda_{mk}U_N(z_s)\\ \lambda_{mk}U_N(z_f)\\ T_N(z_f)\\ \lambda_{mk}U_N(z_q)\end{bmatrix}=\begin{bmatrix}-1 & N_{11}^{j2:kf} & 0 & 0\\ 0 & N_{21}^{j2:kf} & -1 & 0\\ 0 & -1 & N_{12}^{kf:q} & N_{11}^{kf:q}\\ 0 & 0 & N_{22}^{kf:q} & N_{21}^{kf:q}-E_{22}^N(E_{12}^N)^{-1}\end{bmatrix}^{-1}\times\begin{bmatrix}-N_{12}^{j2:kf}T_N(z_{s+})\\ -N_{22}^{j2:kf}T_N(z_{s+})\\ 0\\ 0\end{bmatrix} \tag{33}$$

$$\begin{bmatrix}\boldsymbol{U}(z_s)\\ \boldsymbol{U}(z_f)\\ \boldsymbol{T}(z_f)\\ \boldsymbol{U}(z_q)\end{bmatrix}=\begin{bmatrix}-\boldsymbol{I} & \boldsymbol{S}_{11}^{j2:kf} & \boldsymbol{0} & \boldsymbol{0}\\ \boldsymbol{0} & \boldsymbol{S}_{21}^{j2:kf} & -\boldsymbol{I} & \boldsymbol{0}\\ \boldsymbol{0} & -\boldsymbol{I} & \boldsymbol{S}_{12}^{kf:q} & \boldsymbol{S}_{11}^{kf:q}\\ \boldsymbol{0} & \boldsymbol{0} & \boldsymbol{S}_{22}^{kf:q} & \boldsymbol{S}_{21}^{kf:q}-\boldsymbol{E}_{22}\boldsymbol{E}_{12}^{-1}\end{bmatrix}^{-1}\times\begin{bmatrix}-\boldsymbol{S}_{12}^{j2:kf}\boldsymbol{T}(z_{s+})\\ -\boldsymbol{S}_{22}^{j2:kf}\boldsymbol{T}(z_{s+})\\ \boldsymbol{0}\\ \boldsymbol{0}\end{bmatrix} \tag{34}$$

Notice that the traction coefficients on the lower side of the source level z_{s+} can be expressed by those on the upper side and the given discontinuity source. We also mark that the following more complicated problems can be also solved based on the DVP and FBS system of vector functions: (1) the mixed boundary-value problem in soil-structure interaction[5], (2) the layered structures with imperfect interface[25,26], (3) general dislocations in layered flat Earth[18], (4) poroelastic deformation in layered half-spaces[31], and (5) layered smart structures[32].

For general anisotropy, one could just apply the 2D Fourier integral transform or 2D Fourier series approach. Then, the mathematically elegant and computationally powerful Stroh formalism can be used to derive the first-order differential system of equations[33,34]. The Stroh formalism is formed by using both the displacements and tractions expansion coefficients as the unknown functions in each layer, just as we are using the displacement and traction coefficients U_L, U_M, U_N, and T_L, T_M, T_N here.

For the FBS-based method, we can further apply Kummer transformation to substantially reduce the computational cost. As studied in Ref.[18], for example, for a given accuracy, the direct summation may need more than 100000 terms (or 100000 individual Love numbers); with Kummer transformation where the exact asymptotic solution is utilized, one needs

only about 1000 or less terms.

3 Applications

To illustrate the advantages of the proposed approach, we carry out three examples with applications. These are faulting (or dislocation) in a layered earth, soil-structure interactions, and transient waves in near-surface earth profiles. In these examples, we assume the following 4-layer TI elastic half-space as listed in Tab.1. However, the source/loading and responses are different, with further the thickness being in hundred kilometers in Example 1, as defined in Fig.1. In Example 2 and Example 3 below for the time-harmonic cases, a small damping factor $\beta=0.02$ is used so that the original elastic stiffness c_{ij} is replaced by $c_{ij}(1+i\beta)$ where i is the symbol for the imaginary part of a complex variable.

Tab. 1 Thickness in meter, stiffness c_{ij} in GPa, density in kg/m^3

Layer#	Thickness	c_{11}	c_{12}	c_{13}	c_{33}	c_{44}	Density
1	0.15	0.92	0.40	0.46	1.73	0.50	2400
2	0.36	0.20	0.10	0.12	0.60	0.15	2200
3	0.18	0.10	0.05	0.57	0.25	0.70	2000
4	∞	0.23	0.19	0.19	0.23	0.22	1600

Notice: In Example 1 on dislocations in the layered Earth, the thickness unit is in hundred km, instead of m. Furthermore, the problem is static so that density is not needed.

3.1 A finite fault in a layered half-space

In this Example 1, we simulate the co-seismic (i. e., static) deformation, i. e. 3D displacement, on the surface due to a rectangular fault which is located in layer 2 as shown in Fig.1(a). The parameters of the Earth model are listed in Table 1 with the thickness being in hundred kilometers instead of meters. The parameters of the fault are as follows: the left-lower corner is on the z-axis with depth at 50 km, the strike angle is 90° (i. e. along x-axis), dip angle (denoted by δ) is 50° and rake angle (denoted by β) is 10°, the length and width are, respectively, 50 km and 30 km.

It is known that, in a TI medium, an arbitrary fault (dislocation) is a linear combination of four independent ones: vertical strike slip, vertical dip slip , horizontally tensile fracture and vertically tensile fracture[31]. Fig.2 shows the Green's functions (GFs) of these four types (denoted by 12, 32, 22, 33 respectively for the dilatational deformation, and by 12^t and 32^t for the toroidal deformation) for the source depth at 50 km. In computing GFs, we set $R=5000$ km which is sufficiently large. Beyond the circle with radius being 5000 km, the deformation is safely assumed zero. To assure the convergence of the GFs, we sum up about 1000 zeros (i.e., the series is truncated

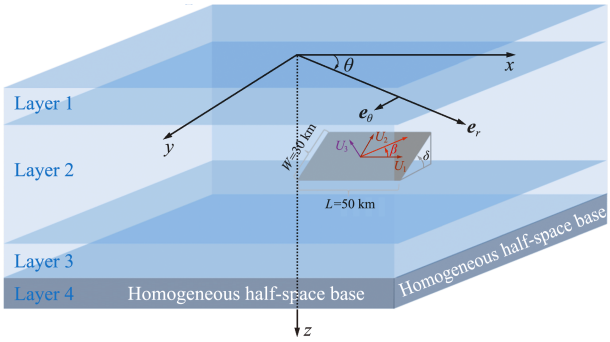

(a) A general finite fault in a four-layer Earth with distance in kilometers. The parameters of the fault are as follows: the left-lower corner of the fault is on the z-axis with depth at 50 km, the strike angle is 90° (i.e., along x-axis), dip angle (denoted by δ) is 50° and rake angle (denoted by β) is 10°, the length and width are, respectively, 50 km and 30 km

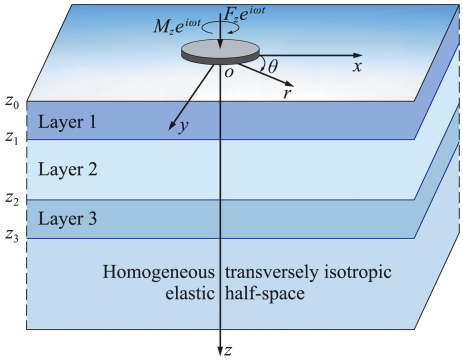

(b) A generally loaded rigid disc on the 4-layer TI elastic half-space

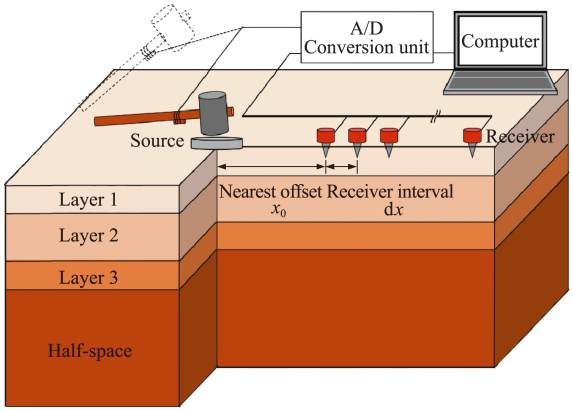

(c) Surface waves survey with 24 geophones and earth profile inverse in the 4-layer TI elastic half-space

Fig. 1 Three typical numerical examples

at about 1000). Notice that since we can pre-calculate the discrete expansion coefficients or the Love numbers, the calculation time is thousands of times faster than the traditional Hankel transform method if 1000 field points are required to draw the curves in Fig.2.

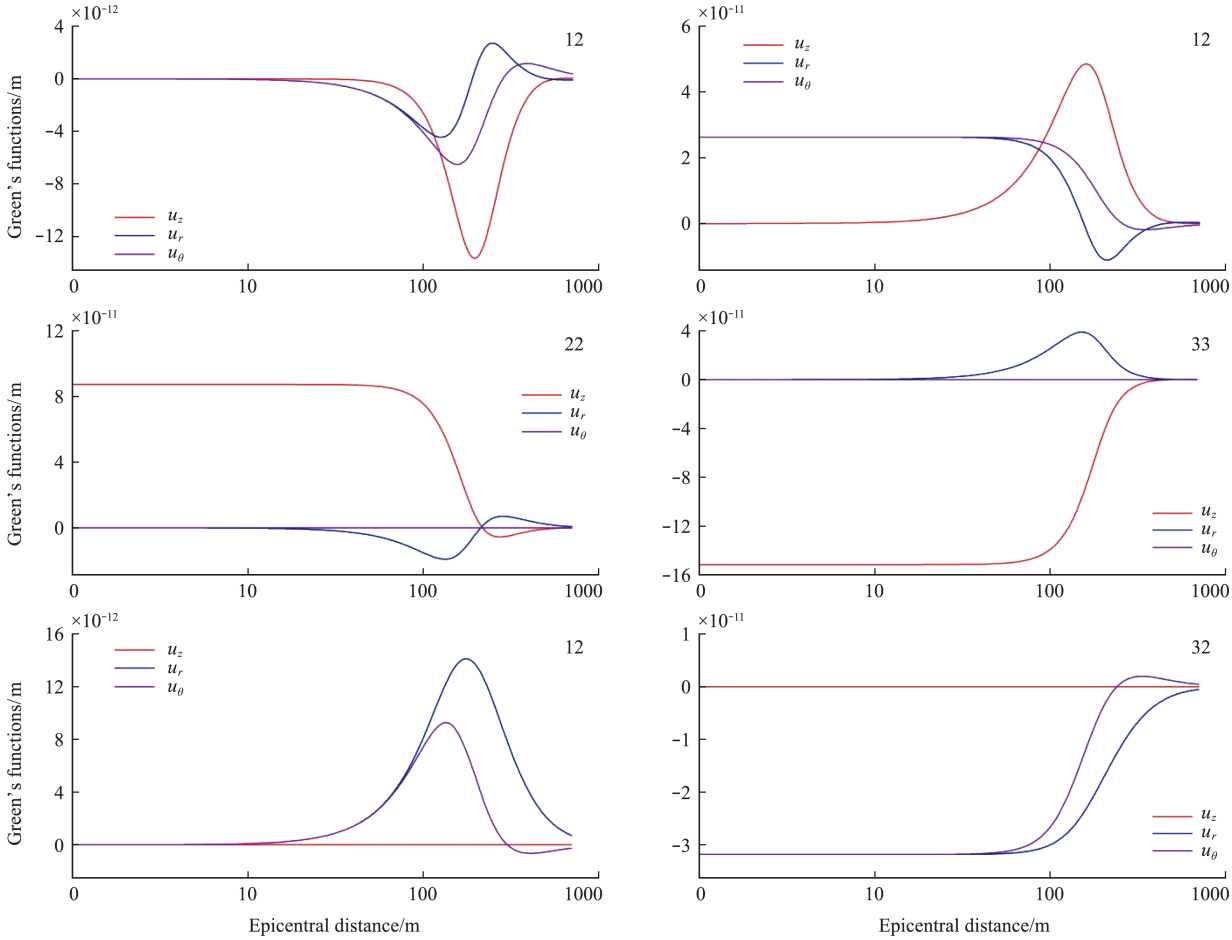

Fig. 2　Green's functions (in meters) of four independent types of dislocation with source depth at 50 km

In computing displacements by using the Green's functions, we need to first approximate the fault by patches. For instance, we use 375 patches where each patch has a size of 2 km × 2 km with a uniform slip of 1 m. This means that this fault causes an earthquake with magnitude being about Mw=5.5. Then, we sum up the deformation due to all the patches to obtain the final results. If we use a total of 7200 field points within the 100 km × 100 km square to calculate the 3D displacement contours, the present method is then at least 7200 times faster than the traditional numerical integral approach.

3.2　Vertical disc loading over a layered half-space

This Example 2 is to illustrate the application of the proposed method in dynamic soil-structure interaction in the four-layer TI elastic half-space, as shown in Fig.1(b). To understand the soil-structure interaction, one needs the fundamental compliance or stiffness matrix when a generally loaded rigid disc is applied on the surface of or within the layered half-space (e.g., Ref. [5]). Under the general load as shown in Fig.1(b), the following equation defines the soil-structure interaction stiffness matrix [K][5,30]

$$\begin{bmatrix} F_x \\ M_y \\ F_y \\ M_x \\ F_z \\ M_z \end{bmatrix} = \begin{bmatrix} K_{HH} & K_{HM} & 0 & 0 & 0 & 0 \\ K_{MH} & K_{MM} & 0 & 0 & 0 & 0 \\ 0 & 0 & K_{HH} & -K_{HM} & 0 & 0 \\ 0 & 0 & -K_{MH} & K_{MM} & 0 & 0 \\ 0 & 0 & 0 & 0 & K_{VV} & 0 \\ 0 & 0 & 0 & 0 & 0 & K_{TT} \end{bmatrix} \begin{bmatrix} u_{x0} \\ \theta_{y0} \\ u_{y0} \\ \theta_{x0} \\ u_{z0} \\ \theta_{z0} \end{bmatrix} \tag{37}$$

where the left-hand side is the applied load (force F_i and moment M_i) on the disc, and the column matrix on the right-hand side are the displacements (displacements u_i and rotations θ_i) below the disc

induced by the applied load.

The soil-structure interaction is mathematically a complicated mixed boundary-value problem. Taking the vertical loading F_z as an example in which F_z is applied on the rigid disc of radius $r=a$ on the surface. For this case, the boundary condition on the surface $z=0$ of the layered half-space (for frictionless contact and independent of coordinate θ) is

$$\begin{aligned} u_z(r,0) &= u_{z0} \quad (0 \leqslant r \leqslant a) \\ \sigma_{zz}(r,0) &= 0 \quad (a \leqslant r < \infty) \\ \sigma_{rz}(r,0) &= 0 \quad (0 \leqslant r < \infty) \end{aligned} \tag{38a}$$

where u_{z0} in Eq.(38a) is unknown which needs to be determined by the vertical force balance between the applied F_z and the vertical traction σ_{zz} under the disc, given by

$$2\pi \int_0^a \sigma_{zz}(r,0)\, r\mathrm{d}r = F_z \tag{38b}$$

To solve this complicated mixed boundary-value problem, we propose to find the Green's functions due to the uniform vertical load within the ring area on the surface where the uniform load density is unknown, to be determined by the force balance relation Eq.(38b). Then, an integral least-square approach is applied to find u_{z0} in Eq.(38a)[30]. Finally, the relationship Eq.(38b) between the applied F_z and the displacement under the disc can be found, which solves one of the required soil-structure interaction stiffness elements.

Fig.3 shows the convergence of this stiffness element as a function of ring number. $|\ |$ denotes the module of the normalized stiffness. The normalized stiffness and frequency are respectively defined as $K^*_{VV}=K_{VV}/(c_{44}\,a)=F_z/(u_{z0}\,c_{44}\,a)$ and $\omega_0=\omega a\sqrt{\rho/c_{44}}$, in which $c_{44}=0.9$ GPa and $\rho=2400$ kg/m^3. As can be seen that when N_r is greater than 24, the corresponding results in both static ($\omega_0=0$) and dynamic cases show good convergence. Consequently, we take $N_r=36$ in the associated calculation to ensure the accuracy of the results. We also compare the vertical stiffness from the present method with those based on the CSVF method for different input frequencies. For instance, for $\omega_0=0$ and $N_r=36$, $|K^*_{VV}|=1.790$ (present) and $|K^*_{VV}|=1.786$ (CSVF), with a relative error 0.22%; for $\omega_0=4$ and $N_r=36$, $|K^*_{VV}|=22.160$ (present) and $|K^*_{VV}|=22.148$ (CSVF), with a relative error 0.05%. However, the computational time of present method for a given frequency and with $N_r=36$ took only about 1 minute, while the CSVF method required about 60 minutes (in the same laptop PC). That is to say, the computational efficiency of the present method is at least 60 times faster than the CSVF method.

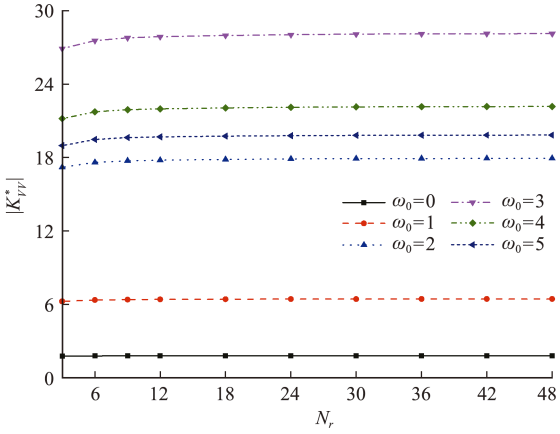

Fig. 3 Convergence of the normalized vertical stiffness with different ring number N_r($M=100000$, $R/a=650$), for different normalized frequencies

3.3 Surface waves in a layered half-space

In this Example 3, surface waves in the four-layer half-space are analyzed. Waveforms on the surface of the layered half-space are particularly useful in the inversion of shear velocity profile[17,35]. For instance, in the multichannel analysis of surface waves (MASW)[36], time-domain vertical and horizontal displacements can be recorded and converted to the dispersion curves to compare with the modeling results. Such comparison would help refine or invert the true velocity profiles in the layered half-space. As such, calculations of full waveforms, dispersion curves and the corresponding modal shapes are all important in the forward modeling.

Shown in Fig.4 are the vertical and horizontal displacement waveforms on the surface of the four-layer TI elastic half-space induced by a uniform vertical surface load. Here, 24 channels on the surface (with nearest offset $x_0=0.2$ m and spacing $\mathrm{d}x=0.2$ m) are used. The source is

applied within a circle of diameter $2a=0.1$ m, and in terms of times, as a half-sine pulse with duration $T_p=0.025$ s, expressed as $\sin(\pi t/T_p)$. In the simulation, the parameter $R=500$ m was used, along with truncation terms at $M=10000$. When presenting the time-domain surface displacements, we fixed $\mathrm{d}t=0.0005$ s, $T=0.25$ s (number of time-domain data $=500$, $\mathrm{d}f=4$ Hz, Nyquist frequency$=10000$ Hz).

Since, for a given frequency, the calculation has to be carried out for the 24 channels (or 24 field points) on the surface, the FBS-based method is at least 24 times faster than the Hankel transform-based numerical quadrature. Then, in the time-domain, the computational efficiency would be 24 times the number of frequencies used for inverse Fourier transform. This number is 250 in Example 3. As such, the FBS-based method is more advanced than the existing numerical quadrature methods.

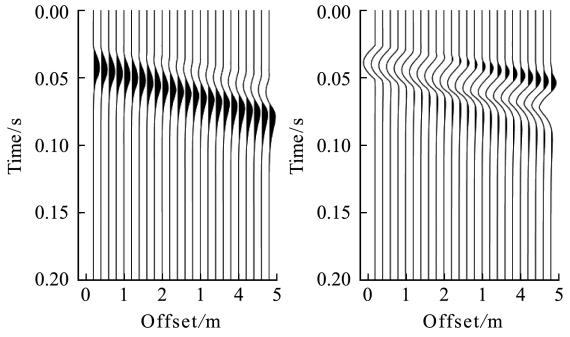

Figu.4　Vertical $u_z(r,t)$ and horizontal $u_r(r,t)$ waveforms obtained from 24 channels induced by a half-sine pulse, where the nearest offset is fixed at $x_0=0.2$ m with fixed space $\mathrm{d}x=0.2$ m, where 250(=500/2) frequencies are used to obtain the time-domain results

4　Conclusions

We have presented an advanced computational approach for modeling layered structures along with three examples of applications: faulting (or dislocation) in a layered earth, soil-structure interactions, and transient waves in near-surface earth profiles. This approach is based on the Fourier-Bessel series (FBS) system of vector functions and the dual-variable and position (DVP) method. While the examples presented are for the purely elastic media showing computational advantages as compared to the existing conventional approaches, this approach can be extended to many other more complicated and coupled material systems, with some of them being under investigation.

Acknowledgments

The first author (E.Pan) has benefitted a lot from Prof. WX Zhong's precision integration method, and from Prof.G.Lin's research on soil-structure interaction. He would also like to thank Prof. GD Cheng's invitation to contribute to this special issue.

References:

[1] Vinyas M, Kattimani S C. Finite element evaluation of free vibration characteristics of magneto-electro-elastic rectangular plates in hygrothermal environment using higher-order shear deformation theory [J]. *Composite Structures*, 2018, **202**: 1339-1352.

[2] Garg N, Saputra A, Donough M, et al. Application of scaled boundary finite element method for three-dimensional modeling of bi-axial bending in thick laminated composite plates [J]. *Mechanics of Advanced Materials and Structures*, 2022, **29**(27): 6935-6947.

[3] Pan E N. Green's functions for geophysics: Areview [J]. *Reports on Progress in Physics*, 2019, **82**(10): 106801.

[4] Luco J E, Westmann R A. Dynamic response of circular footings [J]. *Journal of the Engineering Mechanics Division*, 1971, **97**(5): 1381-1395.

[5] Lin G, Han Z J, Li J B. An efficient approach for dynamic impedance of surface footing on layered half-space [J]. *Soil Dynamics and Earthquake Engineering*, 2013, **49**: 39-51.

[6] Ai Z Y, Liu C L, Jiang J P. Dynamic analysis of a vertically loaded rigid disc in a transversely isotropic multilayered half-space [J]. *Meccanica*, 2016, **51**(8): 1887-1895.

[7] Keawsawasvong S, Senjuntichai T. Vertical dynamic response of rigid circular foundation in multilayered transversely isotropic poroelastic half-space [J]. *International Journal of Structural Stability and Dynamics*, 2021, **21**(9): 2150124.

[8] Pan E. Static response of a transversely isotropic and layered half-space to general surface loads [J]. *Physics of the Earth and Planetary Interiors*, 1989, **54**(3-4): 353-363.

[9] Pan E. Static response of a transversely isotropic and

layered halfspace to general dislocation sources[J]. *Physics of the Earth and Planetary Interiors*, 1989, **58**(2-3): 103-117.

[10] Pan E. Thermoelastic deformation of a transversely isotropic and layered half-space by surface loads and internal sources[J]. *Physics of the Earth and Planetary Interiors*, 1990, **60**(1-4): 254-264.

[11] Ratnanather J T, Kim J H, Zhang S R, et al. Algorithm 935: IIPBF, a MATLAB toolbox for infinite integral of products of Bessel functions [J]. *ACM Transactions on Mathematical Software*, 2014, **40**(2): 1-12.

[12] Lucas S K. Evaluating infinite integrals involving products of Bessel functions of arbitrary order[J]. *Journal of Computational and Applied Mathematics*, 1995, **64**(3): 269-282.

[13] Lucas S K, Stone H A. Evaluating infinite integrals involving Bessel functions of arbitraryorder [J]. *Journal of Computational and Applied Mathematics*, 1995, **64**(3): 217-231.

[14] Al-Khoury R, Scarpas A, Kasbergen C, et al. Spectral element technique for efficient parameter identification of layered media. I. Forward calculation[J]. *International Journal of Solids and Structures*, 2001, **38**(9): 1605-1623.

[15] Doyle J F. *Wave Propagation in Structures: Spectral Analysis Using Fast Discrete Fourier Transforms* [M]. New York: Springer, 1997.

[16] Han Z, Yang L, Fang H, et al. Dynamic simulation of falling weight deflectometer tests on flexible transversely isotropic layered pavements[J]. *Soil Dynamics and Earthquake Engineering*, 2020, **139**: 106353.

[17] Lin C P, Wu T J, Pan E N. An efficient full-wavefield computational approach for seismic testing in a layered half-space [J]. *Soil Dynamics and Earthquake Engineering*, 2022, **161**: 107423.

[18] Zhou J C, Pan E N, Lin C P. A novel method for calculating dislocation Green's functions and deformation in a transversely isotropic and layered elastic half-space [J]. *Engineering Analysis with Boundary Elements*, 2023, **152**: 22-44.

[19] Zhou J, Pan E, Bevis M. A point dislocation in a layered, transversely isotropic and self-gravitating Earth. Part IV: Exact asymptotic solutions of dislocation Love numbers for the special case of isotropy[J]. *Geophysical Journal International*, 2021, **225**(1): 664-683.

[20] Pan E N, Lin C P, Zhou J C. Fundamental solution of general time-harmonic loading over a transversely isotropic, elastic and layered half-space: An efficient and accurate approach[J]. *Engineering Analysis with Boundary Elements*, 2021, **132**: 309-320.

[21] Thomson W T. Transmission of elastic waves through a stratified solid medium [J]. *Journal of Applied Physics*, 1950, **21**(2): 89-93.

[22] Haskell N A. The dispersion of surface waves on multilayered media[J]. *Bulletin of the Seismological Society of America*, 1953, **43**(1): 17-34.

[23] Kennett B L N. *Seismic Wave Propagation in Stratified Media*[M]. Cambridge: Cambridge University Press, 1983.

[24] Kausel E, Peek R. Dynamic loads in the interior of a layered stratum: An explicit solution[J]. *Bulletin of the Seismological Society of America*, 1982, **72**(5): 1459-1481.

[25] Liu H, Pan E N. Time-harmonic loading over transversely isotropic and layered elastic half-spaces with imperfectinterfaces [J]. *Soil Dynamics and Earthquake Engineering*, 2018, **107**: 35-47.

[26] Liu H, Pan E N. Indentation of a flat-ended cylinder over a transversely isotropic and layered half-space with imperfect interfaces[J]. *Mechanics of Materials*, 2018, **118**: 62-73.

[27] Zhong W X, Lin J H, Gao Q. The precise computation for wave propagation in stratified materials [J]. *International Journal for Numerical Methods in Engineering*, 2004, **60**(1): 11-25.

[28] Tan E L. Hybrid compliance-stiffness matrix method for stable analysis of elastic wave propagation in multilayered anisotropic media[J]. *The Journal of the Acoustical Society of America*, 2006, **119**(1): 45-53.

[29] Zhang Z Q, Pan E N. Time-harmonic response of transversely isotropic and layered poroelastic half-spaces under general buried loads [J]. *Applied Mathematical Modelling*, 2020, **80**: 426-453.

[30] Zhang Z Q, Pan E N. Coupled horizontal and rocking vibrations of a rigid circular disc on the surface of a transversely isotropic and layered poroelastic half-space[J]. *Applied Mathematical Modelling*, 2023, **114**: 270-290.

[31] Zhou J C, Pan E N, Lin C P. Transient Green's functions of dislocations in transversely isotropic and layered poroelastic half-spaces [J]. *Engineering Analysis with Boundary Elements*, 2023, **146**: 155-169.

[32] Nirwal S, Lin C P, Tran Q K, et al. Time-harmonic loading over a piezoelectric layered half-space [J].

Journal of Intelligent Material Systems and Structures, 2023, **33**: 1351-1363.

[33] Vattré A, Pan E N. Thermoelasticity of multilayered plates with imperfect interfaces [J]. *International Journal of Engineering Science*, 2021, **158**: 103409.

[34] Vattré A, Pan E N. Dislocation singularities in layered magneto-electro-elastic plates [J]. *International Journal of Engineering Science*, 2022, **181**: 103765.

[35] Lin C P, Pan E N, Tran Q K, et al. A unified approach for relationships among Green's function, normal modes, and dispersion spectrum in layered elastic half-space, with corrected misconceptions on surface wave dispersion and testing[J]. *Geophysical Journal International*, 2022, **232**(2): 1357-1375.

[36] Park C B, Miller R D, Xia J H. Imaging dispersion curves of surface waves on multi-channel record[A]. SEG Technical Program Expanded Abstracts [C]. 1998.

一种用于层状结构模型的先进计算方法

潘爾年*[1]，　周江存[2]，　林志平[1]，　张智卿[3]

(1. 阳明交通大学 土木工程系 防灾与水环境研究中心，新竹 300；
2. 中国科学院精密测量科学与技术创新研究院，武汉 430077；
3. 温州理工学院 建筑与能源工程学院，温州 325035)

摘　要：提出一种针对层状结构模型的先进计算方法。研究的层状结构通常为水平层状板或者层状半空间，结构由横观各向同性(TI)材料组成，材料对称轴指向分层方向。本文方法可以考虑材料的多场耦合特性，即热弹性、多孔弹性和磁电弹性耦合。基于最近提出的傅立叶-贝塞尔级数(FBS)向量函数系和双变量/位置(DVP)方法，建立了本文的先进计算方法。DVP 能够无条件稳定地将层矩阵从一层传播到下一层。FBS 向量函数系具有以下特点，(1) 反映了具有明确类型的广义变形/波，(2) 将展开系数预先计算为 Love 数，然后将其用于涉及问题的模拟。层状地球中的断层(或位错)作用、土-结构相互作用以及近地表地球剖面中的瞬态波等三个典型算例，证明了提出方法的准确性和有效性。

关键词：分层介质；横向各向同性；傅立叶-贝赛尔级数系统；双变量位置法；多场耦合；勒夫数

中图分类号：O343　　**文献标志码**：A　　**文章编号**：1007-4708(2024)01-0000-11

收稿日期：2023-09-09；**修改稿收到日期**：2023-10-30.

基金项目：台湾科学与技术委员会资助项目(NSTC 111-2811-E-A49-534)；湖北珞珈实验室开放基金(220100033)；台湾科学与技术委员会资助项目(MOST 110-2625-M-A49-004)；国家自然科学基金(52178367)资助项目.

作者简介：潘爾年*(1955-)，男，博士，教授(E-mail: ernianpan@nycu.edu.tw).

引用本文/Cite this paper：

潘爾年，周江存，林志平，等. 一种用于层状结构模型的先进计算方法[J]. 计算力学学报，2024，**41**(1)：167-177.

PAN Er-nian, ZHOU Jiang-cun, LIN Chih-ping, et al. An advanced computational approach for layered structure modeling[J]. *Chinese Journal of Computational Mechanics*, 2024, **41**(1): 167-177.